Show, Tushar Kanti ; Hirdaris, Spyros; Datta, Ranadev

A Fully Coupled Time-Domain BEM-FEM Method for the Prediction of Symmetric Hydroelastic Responses of Ships with Forward Speed

Published in:
Shock and Vibration

DOI:
10.1155/2022/4564769

Published: 08/03/2022

Hindawi
Shock and Vibration
Volume 2022, Article ID 4564769, 18 pages
https://doi.org/10.1155/2022/4564769

Research Article

A Fully Coupled Time-Domain BEM-FEM Method for the Prediction of Symmetric Hydroelastic Responses of Ships with Forward Speed

Tushar Kanti Show,[1] **Spyros Hirdaris**,[1,2] **and Ranadev Datta**[1]

[1]*Indian Institute of Technology Kharagpur, Kharagpur 721302, West Bengal, India*
[2]*Aalto University, School of Engineering, Marine Technology Group, Espoo 02150, Finland*

Correspondence should be addressed to Spyros Hirdaris; spyros.hirdaris@aalto.fi and Ranadev Datta; ranadev@naval.iitkgp.ac.in

Received 24 December 2021; Revised 24 January 2022; Accepted 28 January 2022; Published 8 March 2022

Academic Editor: Shan Gao

This paper presents a direct time-domain method for the prediction of symmetric hydroelastic responses of ships progressing with forward speed in small amplitude waves. A transient time-domain free surface Green function is used for the idealisation of the seakeeping problem using an Earth fixed coordinate system. Free surface ship hydrodynamics are idealised in the time domain by a Green function, and forward speed effects are idealised by a space-state model. Modal actions are accounted for by Timoshenko beam structural dynamics. Flexible fluid structure interaction (FFSI) coupling is enabled by a body boundary condition, and a direct integration Newmark-β scheme is used to obtain symmetric dynamic responses. The method is validated against available published numerical and experimental results. A parametric study for different container ship hull forms confirms that (i) forward speed effects should be taken under consideration as far as practically possible and (ii) hull flexibility effects accounting for hull shear deformation and rotary inertia are more notable for slender hull forms.

1. Introduction

In recent years, the economies of scale lead to increase in the numbers and sizes of large ocean-going vessels. For example, Ultra Large Container Ships (ULCSs) with capacity of more than 20,000 TEU and length and beam exceeding 400 m and 60 m, respectively, is today the norm that challenges the wave load margins introduced by classification rules [1]. Because of the slenderness and open deck configuration, these vessels are prone to springing and whipping-induced loads in stochastic seaways [2]. *Springing* is a phenomenon in which wave frequency or its harmonics are able to resonate at the structural natural frequency and may lead to fatigue failure. *Whipping* results from slamming of ships which causes transient dynamic loading along the hull girder. It is important for structural design as it imparts impact loads leading to fatigue failures [3, 4].

Hydroelastic idealisations used for the prediction of springing and whipping loads can be carried out in the frequency or time domains. "*Frequency-domain*" methods gained popularity since late 70s when the basic hydroelasticity theory combining strip theory and Timoshenko beam dynamics was introduced by Bishop and Price [5]. The three-dimensional version of this method was introduced by Bishop et al. [6]. Their approach combined FEA (for dry analysis) and frequency-domain Green function methods (for the wet analysis). To date, these methods have been applied successfully to a variety of merchant and naval ships, and their capability to simulate symmetric, antisymmetric, and asymmetric dynamic behaviour of ships in waves and for use in design has been widely demonstrated in the literature (e.g., [7–14]).

The concept of frequency-domain modal analysis has been successfully applied not only to describe steady-state responses but also to describe the behaviour of symmetric transient responses due to slamming in irregular seaways [15–17]. Yet, comparisons between 2D time and frequency-domain techniques demonstrated that the effects of nonlinearities become particularly important at higher speeds and for ships with large flare [18]. Since the application of Reynolds-averaged Navier–Stokes computational fluid dynamics (RANS CFD) hydroelastic methods remains computationally time consuming (e.g., [19, 20], potential flow time-domain hydroelastic methods remain preferable for the prediction of the influence of whipping and springing loads for ship design and assessment.

"*Time-domain*" potential flow hydroelastic methods can be divided in two categories, namely, (a) the expanded Cummins' equation method and (b) direct simulation methods. In direct simulation methods, structural dynamics are idealised by finite elements and flexible fluid structure interaction (FFSI) is enabled by a boundary element method (BEM) on the interfacing boundaries (e.g., [21–32]). Although the direct coupling can be beneficial for strongly nonlinear problems, its applications are computationally expensive. On the other hand, the expansion of Cummins' equation method makes use of "*impulse response functions (IRFs)*," Fourier transformation, and structural dynamics and is therefore considered simpler in terms of computational modelling and efficiency (e.g., [33–39]).

Recently, Pal et al. [40, 41] used the 3D time-domain panel method based on time-domain free surface Green's function. The ship structure was modelled as an Euler beam. This work demonstrated that direct coupling hydroelastic methods can be more beneficial for strongly nonlinear problems as they allow for implicit implementation of wet modes and the easier inclusion of hydrodynamic nonlinearities. Weakly nonlinear hydroelasticity methods have also been presented by Kim et al. [26–28] and Jiao et al. [39]. The former used a Rankine panel method to idealise nonlinear hydrodynamics and a simplified finite element for Vlasov beam dynamics. The latter accounted for the influence of Froude–Krylov forces while radiation-diffraction forces were considered linear. Along these lines, it is now understood that Rankine panel or free surface time-domain panel methods are more suitable for inclusion of nonlinear radiation-diffraction forces. Segmented model tests are widely adopted for the measurement of ship hydroelastic motions and loads (e.g., [33, 42–46]). Notwithstanding this, results from model tests remain uncertain and generally unambiguous [47].

Building up from the work by Pal et al. [40], the originality and focus of this work is on exploring the adequacy of time-domain physical assumptions to model forward speed effects and exploring the influence of Timoshenko beam dynamics (rotary inertia and shear deformation effects) on predicting symmetric flexible dynamic response in waves. As explained in Section 2 of the paper, the formulation of the hydrodynamic problem is based on the model of Datta and Sen [48]; forward ship speed effects are idealised by a space-state function and modal actions are accounted for by Timoshenko beam structural dynamics. Flexible fluid structure interaction (FFSI) coupling is enabled by a body boundary condition, and a direct integration Newmark-β scheme is used to obtain symmetric dynamic responses. Results from a time-domain hydroelastic method that are compared for three different modern container ship hull forms and the experiments of Rajendran and Guedes Soares [33] are presented in Section 3. The influence of structural flexibility on ship responses is discussed in Section 4 and conclusions are drawn in Section 5.

2. Theory

Figure 1 presents the case of a flexible ship progressing with uniform forward speed U. The origin $Oxyz$ of the vessel lies in the Earth fixed coordinate system in way of the centre of gravity $G(X_s, Y_s, Z_s)$. The mathematical idealisation presented in the following sections comprises two parts, namely, "*structural dynamic*" and "*hydrodynamic*" idealisations. In the former, FEA-based Timoshenko beam structural dynamics are used to idealise the structural part of the FFSI problem. The boundary integral equation is then formulated using time-domain free surface Green's function, and FFSI coupling is enabled by a direct integration Newmark-β scheme [49].

2.1. Structural Dynamic Idealisation. The structure is assumed to behave as a slender nonuniform Timoshenko beam accounting for shear deformation and rotary inertia effects (see Figure 2) [50]. Transverse shear is assumed to be constant over the cross section. The rotation about the y axis is denoted by an independent function, namely, ψ. The dynamical behaviour of the ship hull due to hydrodynamic external force can be described by governing differential equations. In pure bending, the cross section maintains orthogonality, but in this work, the net slope of the natural axis is presented in terms of both flexure and the shear strain. In this formulation, w and ψ represent independent field variables idealising the transverse deflection of natural fibre and the angle of flexure, respectively. Therefore, the shear strains (ε) and stresses (σ) are, respectively, defined as $\varepsilon = -z$ and $\sigma = -Ez$. The vertical bending moment (M) and shear force (v) are defined as $M = EI$ and $v = GA_c k_s(\psi + dw/dx)$. In these formulations, G presents the modulus of rigidity (shear modulus) and A_s is the effective shear area. As the shear stress is not uniformly distributed over the cross section of the beam, considering uniform area overestimates the stresses. In an actual flexing scenario, the shear force will be lower and the effective shear area is defined as $A_s = A_c k_s$ where A_c is the cross-sectional area and k_s is the shear correction factor with values generally taken as 1.2 (i.e., approximately 80% of the area if considered effective in shear) for classic ship like beam idealisations [5, 51].

The ordinary differential equations expressing the shear forces and bending moments are defined, respectively, by (1) and (2) as

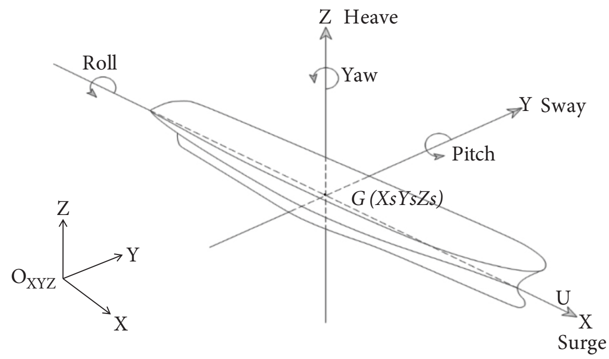

FIGURE 1: Schematic diagram of coordinate systems.

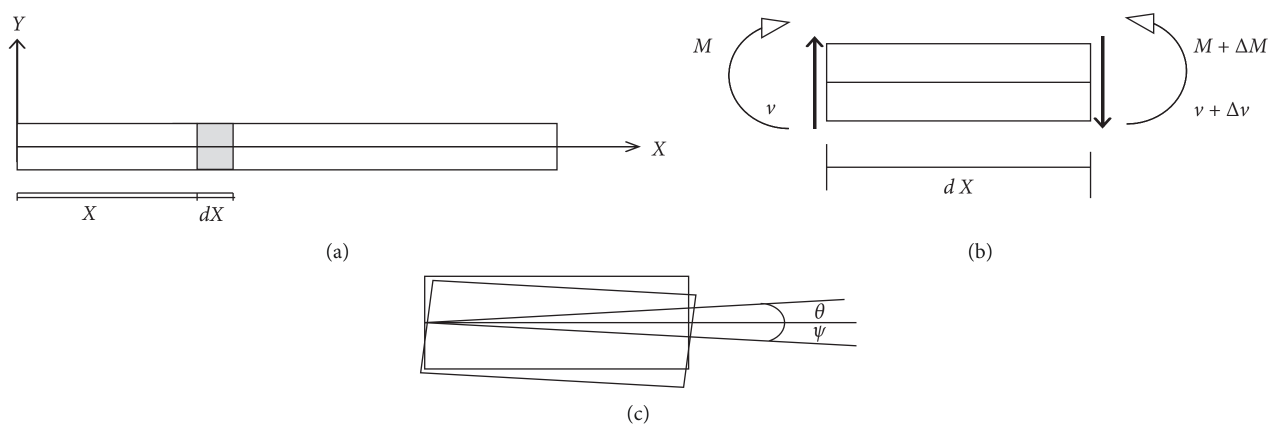

FIGURE 2: Section of a beam representing shear forces (V) and moments (M) at edges.

$$\frac{d}{dx}\left[GA_c k_s\left(\psi+\frac{dw}{dx}\right)\right]+f=0, \tag{1}$$

$$\frac{d}{dx}\left(EI\frac{d\psi}{dx}\right)-GA_c k_s\left(\psi+\frac{dw}{dx}\right)=0. \tag{2}$$

In equation (1), f represents the distributed load over the sectional element of the ship modelled as a beam. The weak form of (1) and (2) can be obtained by introducing two weight functions, namely, transverse deflection w and rotational function ψ, as independent unknowns. A "*Gaussian quadrature method (G-Q)*" can be applied to evaluate the weak form equations as follows:

$$\int_0^{h_e}\left(\frac{dw}{dx}\frac{d\alpha^b}{dx}GA_c k_s\right)dx+\left(\psi\frac{d\alpha^b}{dx}GA_c k_s\right)dx=\int_0^{h_e} f\alpha^b dx+\alpha^b(h_e)Q_1^e+Q_3^e\alpha^b(h_e), \tag{3}$$

$$\int_0^{h_e}\beta^s\frac{dw}{dx}GA_c k_s dx+\int_0^{h_e}\left[\frac{d\beta^s}{dx}\frac{d\psi}{dx}EI+\beta^s\psi GA_c k_s\right]dx=\beta^s(x_A)Q_2^e+Q_4^e\beta^s(h_e). \tag{4}$$

The weak form of the structural dynamic equations (3) and (4) is obtained by introducing two weight function α^b and β^S; h_e is the length of 1D finite element where x_A *an d* x_B are the two consecutive nodes of a beam-like element; Q_1^e and Q_3^e represent elemental shear forces; Q_2^e and Q_4^e denote elemental bending moments. To avoid the shear locking [52], the equations are equally interpolated by a "*reduced integration element (RIE)*." Accordingly, the elemental static equation can be written as

$$\begin{bmatrix} K^{11} & K^{12} \\ K^{21} & K^{22} \end{bmatrix}\begin{Bmatrix} w \\ \psi \end{Bmatrix}=\begin{bmatrix} f_1 \\ f_2 \end{bmatrix}. \tag{5}$$

In (5), the global stiffness (K_{ij}) operators are defined as

$$K_{ij}^{11} = \int_{x_A}^{x_B} GA_c k_s \frac{d\psi_i^{(1)}}{dx}\frac{d\psi_j^{(1)}}{dx} dx, \quad (i = 1, 2, 3, \ldots\ldots n)(j = 1, 2, 3, \ldots\ldots n),$$
$$K_{ij}^{12} = \int_{x_A}^{x_B} GA_c k_s \frac{d\psi_i^{(1)}}{dx}\psi_j^{(2)} dx, \quad (i = 1, 2, 3, \ldots\ldots n)(j = 1, 2, 3, \ldots\ldots n),$$
$$K_{ij}^{21} = \int_{x_A}^{x_B} GA_c k_s \frac{d\psi_i^{(1)}}{dx}\psi_j^{(2)} dx, \quad (i = 1, 2, 3, \ldots\ldots n)(j = 1, 2, 3, \ldots\ldots n),$$
$$K_{ij}^{22} = \int_{x_A}^{x_B} GA_c k_s \psi_i^{(2)}\psi_j^{(2)} dx + \int_{x_A}^{x_B} EI \frac{d\psi_i^2}{dx}\frac{d\psi_j^2}{dx} dx, \quad (i = 1, 2, 3, \ldots\ldots n)(j = 1, 2, 3, \ldots\ldots n). \tag{6}$$

The shear stiffness is computed with one Gauss point. The mass matrix is defined as $[m]_{sb} = [m]_s + [m]_b$, where $[m]_s$ and $[m]_b$ represent the mass matrices for shear and bending criteria, respectively. Therefore, to determine the response history of the beam element, the global finite element equation for dry analysis is expressed as

$$[M]\{\dot{x}\} + [C]\{\dot{x}\} + [K]\{x\} = \{F_{ext}\}. \tag{7}$$

In this equation of motion, the responses of the structure are demonstrated in the form of displacement (x), velocity ($\dot{x}$), and acceleration ($\ddot{x}$); $[M]$ and $[K]$ represent the global mass and stiffness matrices, $[C]$ is the damping matrix, and $\{F_{ext}\}$ is the global external force vector. The formulation presented assumes Rayleigh damping [53] where $[C] = \sigma_d [K] + \varsigma_d [M]$. The value of stiffness proportional coefficient (σ_d) and mass proportional coefficient (ς_d) is taken as presented by Liu et al. [54].

2.2. Hydrodynamic Idealisation. In (7), the external force $\{F_{ext}\}$ vector represents the wave induced loads and moments which may be calculated by solving the hydrodynamic problem. In this study, a 3D time-domain panel method based on transient free surface Green's function has been employed. The theory is formulated based on Earth fixed coordinate system. The complete formulation of the hydrodynamic problem for rigid body case is presented in multiple sources (e.g., [48, 55]). Therefore, the background to the method is only briefly presented here with the aim to explain its relevance for the solution of the hydroelasticity problem. In Figure 3, Ω represents a fluid domain of interest which is surrounded by the free surface S_F, bottom surface S_b, wetted body surface S_0, and the surfaces $S_{-\infty}$, S_∞ at infinity.

The total velocity potential $\phi^T(p,t)$ is defined as

$$\phi^T(p,t) = \phi^I(p,t) + \phi(p,t), \tag{8}$$

where $\phi^I(p,t)$ is the velocity potential of incident waves at any time instant (t) at any arbitrary point p on the fluid domain Ω and $\phi(p,t)$ is the disturbed potential that consists of radiation and diffraction components. Within the context of linear potential theory, solution for $\phi(p,t)$ can be obtained by solving following governing equation:

$$\nabla^2\phi(p,t) = 0, \text{for } p \in \Omega. \tag{9}$$

Using linear free surface boundary condition, body boundary condition, bottom boundary condition, and radiation condition as follows:

$$\begin{aligned}
&\frac{\partial^2\phi}{\partial t^2} + g\frac{\partial\phi}{\partial z} = 0 \text{ at } z = 0,\\
&\frac{\partial\phi}{\partial n} = v_n(x,t) - \frac{\partial\phi^I}{\partial n} \text{ on } S_0,\\
&\frac{\partial\phi}{\partial z} = 0 \text{ on } S_b\\
&\phi, \frac{\partial\phi}{\partial t} = 0 \text{ at } S_\infty
\end{aligned} \tag{10}$$

within the context of rigid body ship dynamics, we can assume that the normal velocity of the body is taken as a function of time. However, if we account for the influence of hydroelasticity, the velocity of the body should be idealised by a state-space function. Considering that the formulation is based on Earth fixed coordinate system, consideration of the so called "*m terms*" [26] is not required. To solve the hydrodynamic problem, transient free surface Green's function is used. The expression for $\phi(p,t)$ becomes

$$\phi(p,t) = -\frac{1}{4\pi}\left\{\begin{aligned} &\iint_{S_0} \sigma(q,t)G^o(p,q)dS + \int_0^t d\tau\left[\iint_{S_0}\sigma(q,t)G_t^f(p,q;t-\tau)dS\right]\\ &-\int_0^\tau d\tau\left[\frac{1}{g}\int_\Gamma \sigma(q,t)G_t^f(p,q;t-\tau)v_N v_n dL\right]\end{aligned}\right\}. \tag{11}$$

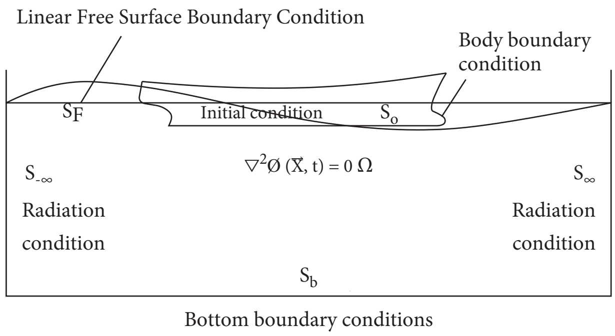

FIGURE 3: Hydrodynamic boundary domain and associated conditions (S denotes surface of relevance to boundary conditions).

The detailed expression for the derivation of (11) is given in Lin and Yue [55]; G^o presents the nonlinear part (Rankine part) of Green's function and G_t^f is the linear part (regular part) of Green's function [56]. This solution produces scattering of velocity potential $\phi(p,t)$ over the surface of the hull; v_N and v_n are normal to the water line Γ and the wetted surface, respectively; $\sigma(p,t)$ represents the strength of the source G; t and τ represent the present and past time increments used in the convolution time integral. The time dependent contribution comes from the second and third integrals that calculate the effect that comes from the disturbance caused in previous time steps. The third integral arises due to the forward speed effects with terms "t" and "τ" denoting the present and past instants in time.

The computation of the velocity potential term $\phi(p,t)$ leads to prediction of dynamic pressure $P(p,t)$ defined as

$$P(p,t) = -\rho_0 \left\{ \phi_t(p,t) - U\phi_x(p,t) + \phi_t^I(p,t) + \frac{1}{2}\left[\nabla\phi(p,t) + \nabla\phi^I(p,t)\right]^2 \right\}. \tag{12}$$

In (12), the density of the fluid is termed as ρ_0. For zero speed, the contribution of quadratic term can be ignored. However, when forward speed effects are accounted for, consideration of quadratic terms is essential. Accordingly, the method is not fully linear and fundamentally different from other time-domain formulations (e.g., [26, 39]). Solving (12) gives the distribution of the pressure at any arbitrary point at any instant of time t. If we assume that $P(\overline{X},t)$ represents the collection of total dynamic pressure at any point on the sectional curve C_{S_x} for an arbitrary vertical section S_x, the sectional force F_{S_x} is defined as

$$F_{S_x} = \int_{C_{S_x}} P(\overline{X},t).\widehat{n}.dC_{S_x}, \tag{13}$$

where $(\overline{n})$ denotes the generalized normal on a section increment (dS_X).

The restoring force $F_i^{restoring}(t)$ at an i^{th} panel of a surface increment ds_i subject to normal $\overline{n}_i$ may expressed as

$$F_i^{restoring}(t) = -\rho_0 g \overline{Z}_i \delta\overline{n}_i.ds_i - \rho_0 g \delta\overline{Z}_i\overline{n}_i.ds_i, \tag{14}$$

where $\overline{Z}_i$ is the water head and δ denotes the leading order variation. Lower-order panel methods assume that variation over a hydrodynamic panel remains constant. As δ varies over the surface, this leading order variation might not be very effective, and therefore Kim et al. [26] proposed the use of a higher-order Rankine panel method. Notwithstanding this, the stability of the numerical idealisation can also be ensured by reducing the size of panels (i.e., using optimum number of fluid domain discretisation) when using a classic Green function method (e.g., [57]).

2.3. Flexible Fluid Structure Interaction (FFSI). Equation (7) may be solved by Newmark [49] time integration method. Accordingly, the nodal displacement vector $\{x\}$ at any time instant t is obtained from the equation

$$\begin{aligned}\left(\frac{[M]}{\alpha\Delta t^2} + \frac{\delta}{\alpha\Delta t}[C] + [K]\right)\{x\}_t &= \{F\}_t + [M]\left[\frac{1}{\alpha\Delta t^2}\{x\}_{t-\Delta t} + \frac{1}{\alpha\Delta t}\{\dot{x}\}_{t-\Delta t} + \left(\frac{1}{2\alpha} - 1\right)\{\ddot{x}\}_{t-\Delta t}\right] \\ &\quad + [C]\left[\frac{\delta}{\alpha\Delta t}\{x\}_{t-\Delta t} + \left(\frac{\delta}{\alpha} - 1\right)\{\dot{x}\}_{t-\Delta t} + \frac{\Delta t}{2}\left(\frac{\delta}{\alpha} - 2\right)\{\ddot{x}\}_{t-\Delta t}\right].\end{aligned} \tag{15}$$

The stability and accuracy of the present numerical scheme during a time increment Δt is dependent on the parameters α and δ. These two parameters also describe the variation of the acceleration over a time step. The numerical values of α and δ in the above equation are in general taken as ¼ and ½, respectively (Kim et al., 2013). The time variations of the acceleration and velocity derivatives are defined as

$$\{\ddot{x}\}_t = \frac{1}{\alpha\Delta t^2}\left(\{x\}_t - \{x\}_{t-\Delta t}\right) - \frac{1}{\alpha\Delta t}\{\dot{x}\}_{t-\Delta t} - \left(\frac{1}{2\alpha} - 1\right)\{\ddot{x}\}_{t-\Delta t}, \tag{16}$$

$$\{\dot{x}\}_t = \{\dot{x}\}_{t-\Delta t} + \Delta t\left[(1-\delta)\{\ddot{x}\}_{t-\Delta t} + \delta\{\ddot{x}\}_t\right]. \tag{17}$$

Accordingly, the velocity and displacement at each section may be obtained from equations (15)–(17). By back substitution in equation (14), the boundary condition for the solution of the fluid problem is obtained and FFSI is enabled.

3. Results

Table 1 outlines the principal particulars of three container ship hulls that have been assessed using the method presented in this publication. The hydrodynamic idealisations for each design and the body plans are shown in Figure 4. The weight and flexural rigidity distributions for all containerships are depicted in Figure 5. Ship 1 is the well-known S175 container ship [46]. Ship 2 is a modern large container ship (LC) design studied under previous ISSC-ITTC benchmarks [3, 33, 58]. Ship 3 is a modern ultra-large container ship (ULC) [59].

The results presented in this paper are given in the nondimensional forms presented in Table 2. Numerical results based on the theory presented in Section 2 are named as TDFlex-T. The computations based on Datta and Soares [41] model are denoted as TDFlex-E, and the results from time-domain rigid body approach of Sengupta et al. [60] are referenced as TDRigid.

3.1. Validation Study. Figures 5(a)–5(d) demonstrate the time history of nondimensional vertical bending moments (VBMs) and shear forces (VSFs) of S175 and ULC at the wave matching region (i.e., $\lambda/L = 1$) for forward speed $F_n = 0.25$. The results presented converge to steady state. This confirms the numerical stability of the solution. In Tables 3–5, dry natural frequencies for the different modes of S175, LC, and ULC are compared against the Euler–Bernoulli models of Rajendran et al. [59] and Rajendran and Guedes Soares [33] as well as the superposition method of Wu and Hermundstad [18]. Variations in the natural frequencies can be attributed to the Timoshenko beam idealisation introduced in Section 2.

In Figure 6, the VBM transfer function for S175 hull at $F_n = 0.25$ is plotted and compared with the numerical method proposed by Datta and Guedes Soares [41] that has been based on an Euler beam model. the experimental results published by Iijima et al. [61]. The differences in the magnitude of the VBM value at the wave matching region ($\lambda/L = 1$) could be attributed to limitations of the linear hydrodynamic theory assumptions and structural idealisations. Notwithstanding this, it is thought that the approach presented captures very well the overall trend of the dynamic response.

Comparisons of results for amidships symmetric responses against [33] are depicted in Figure 7. Figure 7(a) presents a comparison of nondimensional displacement against nondimensional frequency. As shown in Figure 7(b), the magnitude of the VBM matches well with the other published results. Comparison of VBM along the hull for LC is demonstrated in Figure 8 at $F_n = 0.12$. Once again, the results compare well with experiments and the coupled BEM-FEM model given by Datta and Guedes Soares [41].

The VBM at amidships the ULC for $F_n = 0.135$ is shown in Figure 9. Results are compared with experiments by Rajendran et al. [59] and TDFlex-E. Both results underestimate the maximum VBM. However, the overall trend agrees very well with experimental values. It may be therefore concluded that the present numerical model is stable and consistent and captures the symmetric responses with reasonable accuracy.

4. Parametric Study

In this section, a parametric study is carried out to observe the effect of design parameters in symmetric hydroelastic responses such as vertical displacement, VSF, and VBM. The parametric study presented utilises S175 and ULC hulls. Special focus is attributed to the influence of structural rigidity, forward speed, ship length, and slenderness on dynamic response.

4.1. The Influence of Structural Rigidity. The vertical displacement RAO at midships and transfer functions of VSF at $+L/4$position from the aft of the ULC were compared between the flexible and rigid structures for $F_n = 0.135$. Figure 10 shows the comparison of the displacement response amplitude operator (RAO) for rigid and flexible structures over the nondimensional frequency $\omega\sqrt{L/g}$. Observed differences demonstrate that rigid body assumptions overestimate the structural responses. As shown in Figure 11, near the resonating frequency, the ship is likely to experience larger shear forces, which can only be captured if structural flexibility is taken into account. While TDFlex-T is capable of capturing this phenomenon, TDRigid fails to capture the same phenomenon. This implies the importance of capturing the influence of structural flexibility for slender vessels.

4.2. The Influence of Forward Speed. Figures 12(a), 12(b), 13(a), and 13(b) represent the VBM and VSF for S175 hull and the ULC hull, respectively, for different Froude numbers ($F_n = 0.135$, 0.2 , and 0.25). The VBM and VSF results are plotted against the nondimensional frequency $\omega\sqrt{L/g}$. It is observed that the peak symmetric loads drop rapidly with respect to the frequency. This implies that the chances of damage of the structure are higher at lower Froude number at lower frequency zone.

Table 1: General particulars of different container ship models.

General particulars		Ship type		
Notation (unit)	Item	S175	LC	ULC
L_{PP} (m)	Length between perpendiculars	175.0	286.6	333.43
B (m)	Beam	25.4	40.0	42.8
D (m)	Depth	11.0	24.2	27.3
T (m)	Draft	9.5	11.98	13.1
M (tonne)	Total mass	24560.0	85562.7	$1.25e+05$
LCG (m)	Longitudinal centre of gravity	2.78	4.9	4.7
k_{xx} (m)		10.16	14.4	16.94
k_{yy} (m)	Radii of gyration along longitudinal (xx); transverse (yy); and vertical (zz) axes	42.8	70.144	83.9
k_{zz} (m)		43.0	11.412	84.1

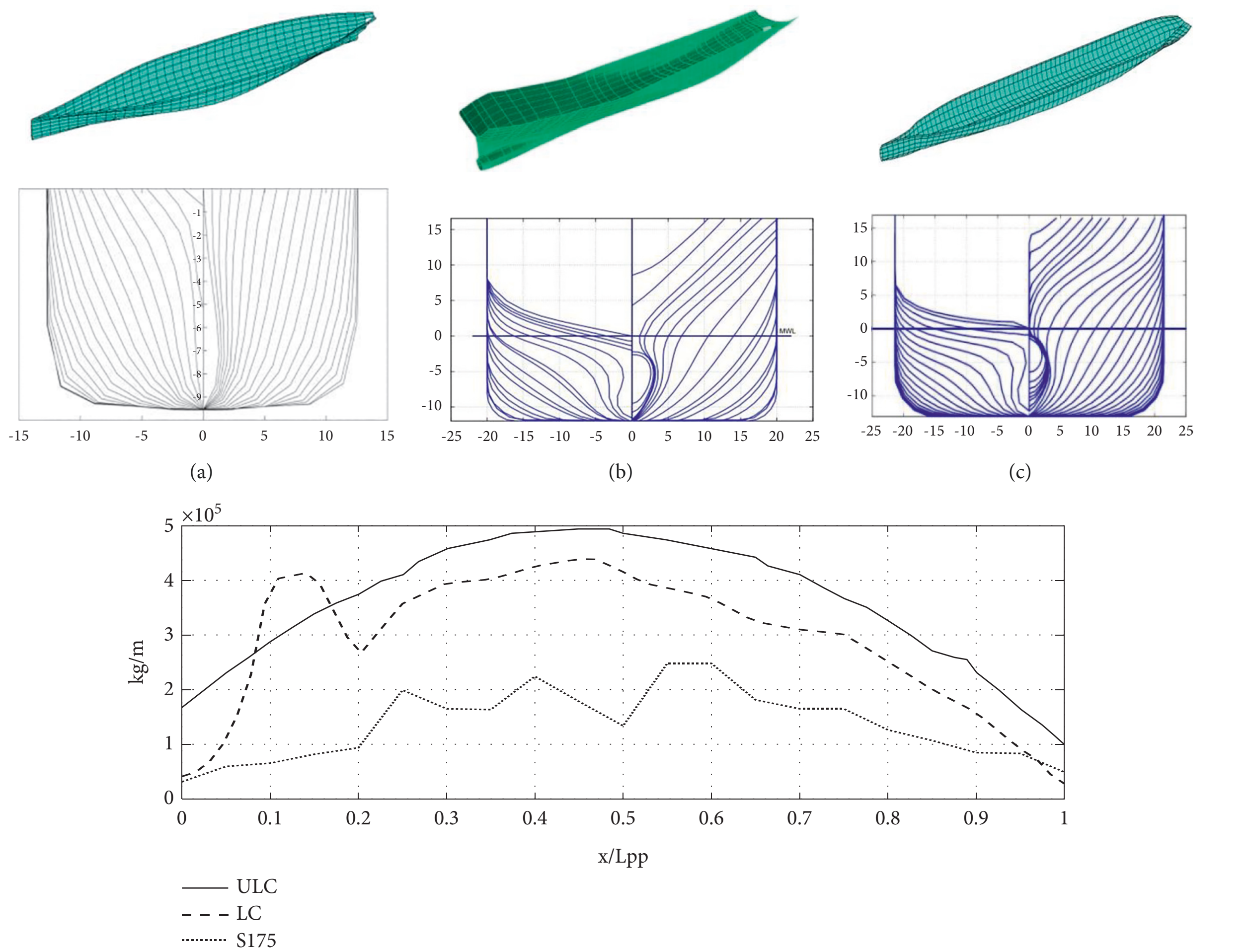

(d)

Figure 4: Continued.

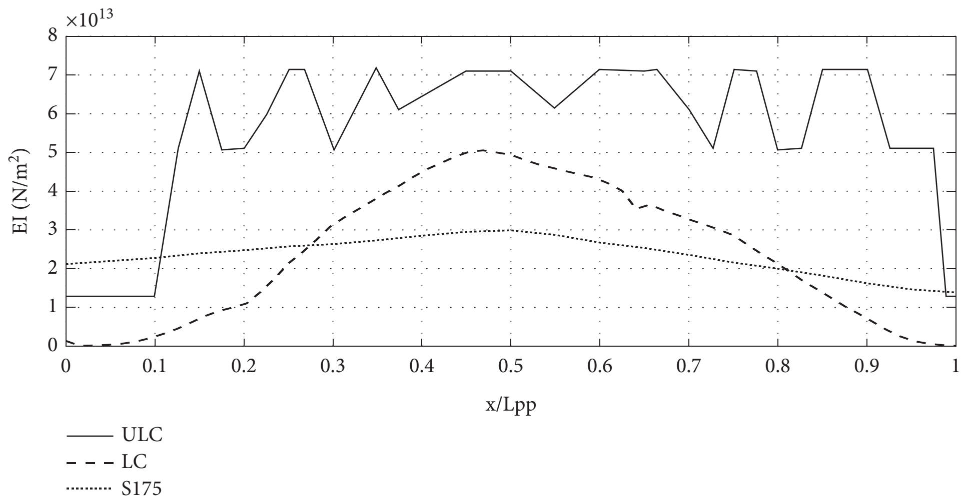

(e)

Figure 4: Body plan and hydrodynamic idealisations for different container ship models. (a) Ship 1: S175. (b) Ship 2: LC. (c) Ship 3: ULC. (d) Mass distributions. (e) Flexural rigidity distributions.

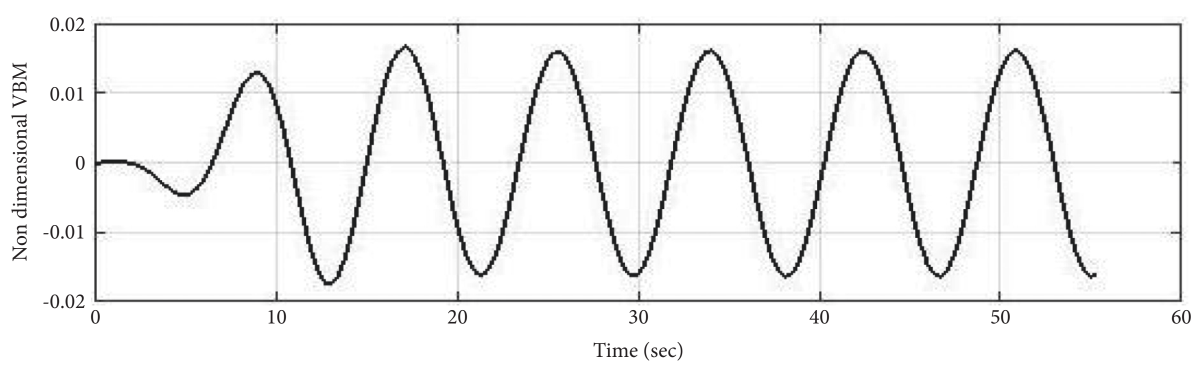

(a)

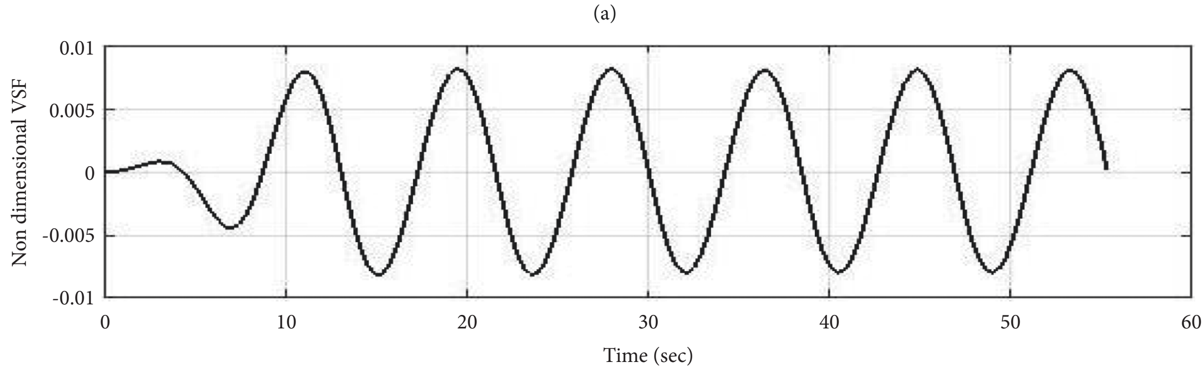

(b)

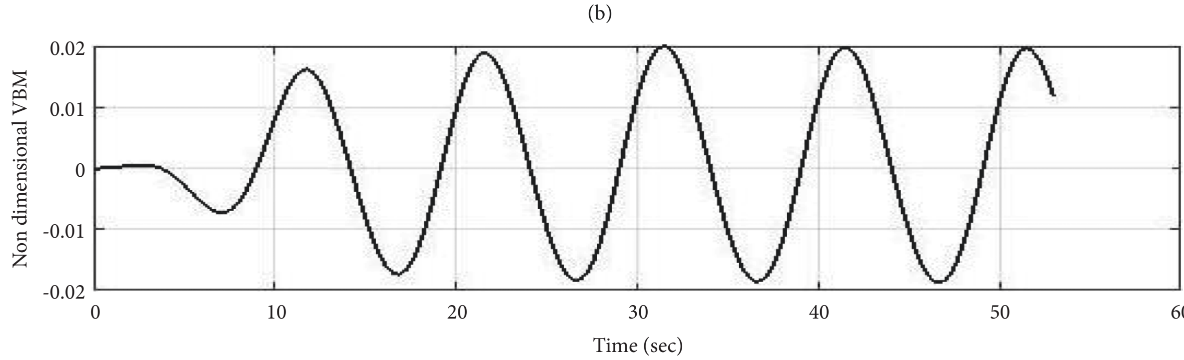

(c)

Figure 5: Continued.

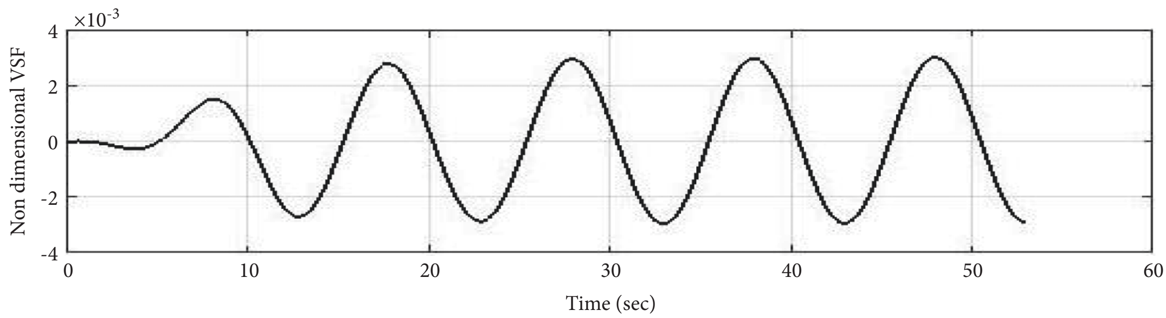

(d)

Figure 5: Symmetric load time histories for ULC and S175 container ships (F_n = 0.25, λ/L = 1). (a) VBM time history, S175. (b) VSF time history, S175. (c) VBM time history, ULC. (d) VSF time history, ULC.

Table 2: Nondimensional dynamic response parameters.

Parameters	Nondimensional format
Frequency (Hz)	$\omega\sqrt{\mathbf{L}/\mathbf{g}}$, $\lambda/\mathbf{L}$
Time (sec)	$\mathbf{t}/\mathbf{T}$
Vertical response (m)	$\lvert\mathbf{x}_3\rvert/\mathbf{A}$
Length along the horizontal axis	x/L
VSF (N/m^2)	$V/(\rho_0 gAL^2)$
VBM (N-m)	$M/(\rho_0 gAL^3)$

Table 3: Dry natural frequencies of the S175 for vertical flexural vibrations.

Mode no.	TDFlex-T (Hz)	Wu and Hermundstad [18] (Hz)	Difference (%)
1	0.3002	0.3024	−0.737
2	0.7299	0.7669	−0.950
3	1.3981	1.4006	−0.170

Table 4: Dry natural frequencies of the LCS for vertical flexural vibrations.

Mode no.	TDFlex-T (Hz)	Rajendran and Guedes Soares [33] (Hz)	Difference (%)
1	0.625	0.64	−2.343
2	1.603	1.64	−2.256
3	3.086	3.11	−0.772

Table 5: Dry natural frequencies of the ULCS for vertical flexural vibrations.

Mode no.	TDFlex-T (Hz)	Rajendran et al. [59] (Hz)	Difference (%)
3	0.717	0.72	−0.416
4	1.864	1.89	−1.37
5	3.527	3.64	−3.10

4.3. The Influence of Ship Length. VSF values for the ULC decrease rapidly at around $\omega\sqrt{L/g} = 2$ and then increase (see Figure 14). This could be attributed to the influence of resonance phenomena. On the other hand, the VSF values for the S175 hull decrease slowly and do not show any secondary peak in the response (see Figures 14–16). This nature of the transfer function of the VSF values for the S175 hull is similar to the rigid body case. It may therefore be concluded that hydroelasticity effects may be more prominent for more slender vessels.

4.4. The Influence of Structural Flexibility on Hydrodynamic Pressure Distributions. The influence of flexibility on local pressure variation was evaluated at the free surface and the hull bottom in way of the bow, stern, and amidships for F_n = 0.25 and λ/L = 1 (see Figure 17). This is because these conditions were shown to be critical in terms of flexible fluid structure interactions (see Section 4).

The variations of nondimensional hydrodynamic pressures over time are shown in Figures 18–20. Figures 18(a)

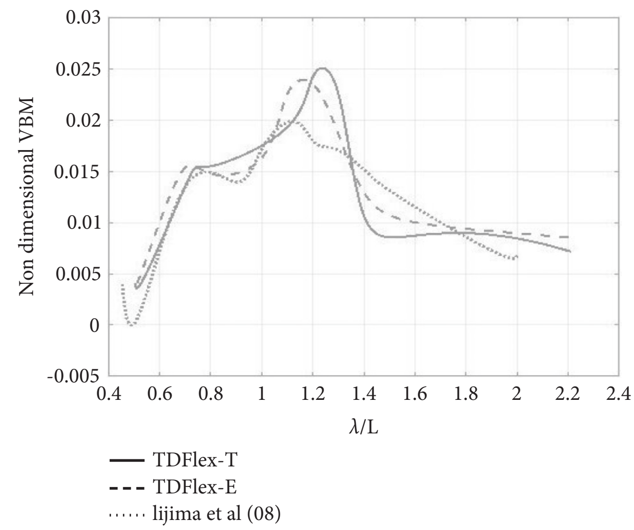

Figure 6: VBM transfer function at midship of S175 (F_n = 0.25).

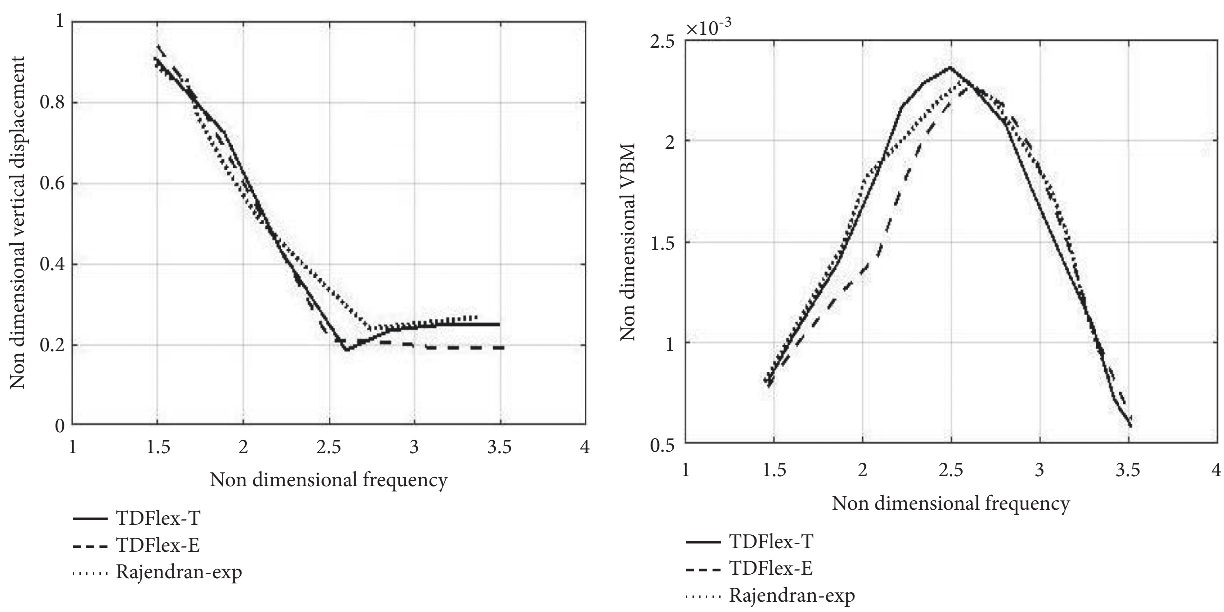

(a) (b)

Figure 7: Symmetric responses, LC (at $F_n = 0$). (a) Vertical displacement. (b) VBM.

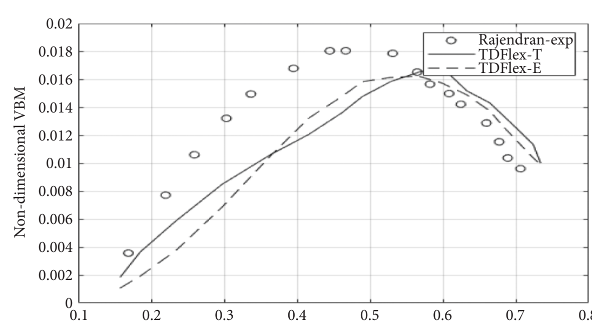

Figure 8: VBMs along the length for LC (F_n = 0.12 and λ/L = 1.06).

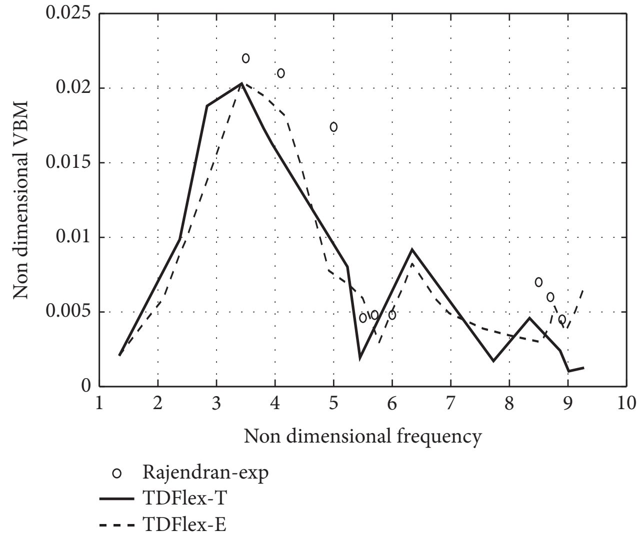

Figure 9: Comparison of rigid body and hydroelastic RAO of vertical deflection for the ULC at L/4.

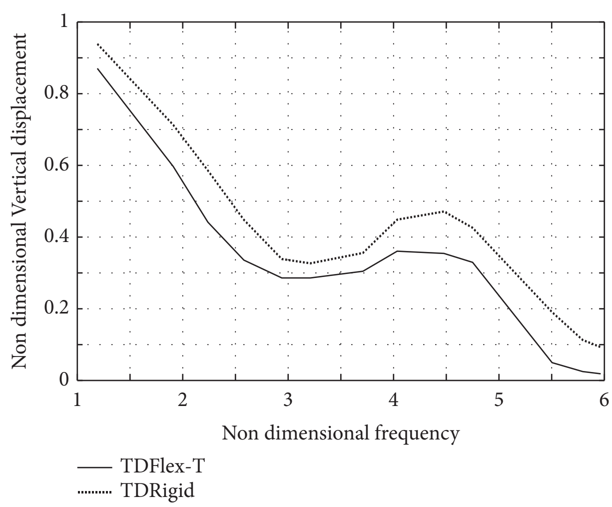

Figure 10: RAOs for vertical displacement for flexible body and rigid body, ULC.

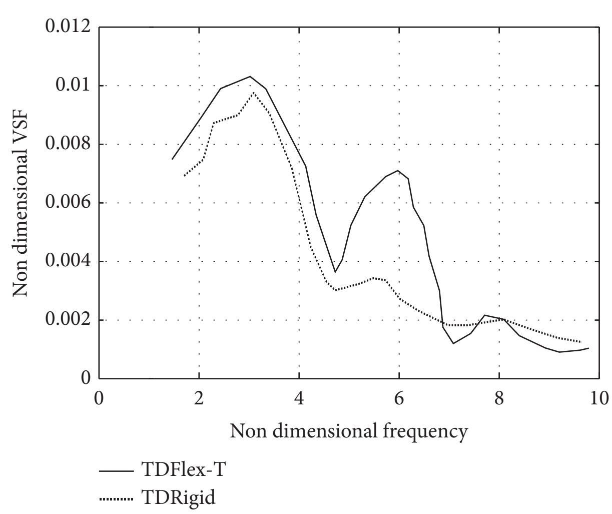

Figure 11: Comparison of rigid body and hydroelastic RAO of VSF for the ULC at L/4.

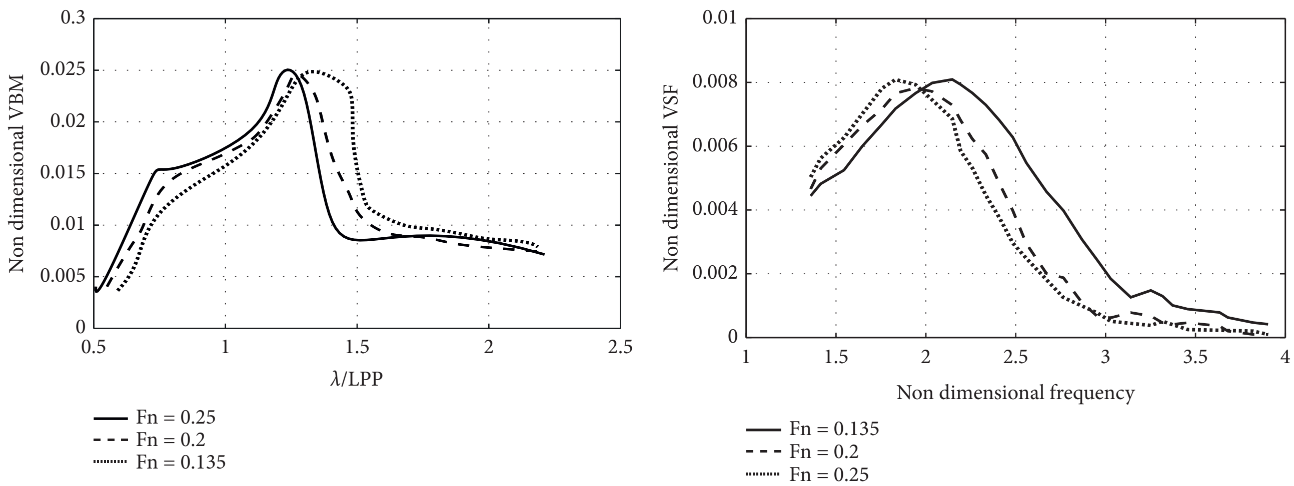

(a) (b)

Figure 12: (a) Transfer function for VBM at amidships for different forward speeds of S175. (b) Transfer function for VSF at amidships for different forward speeds of S175.

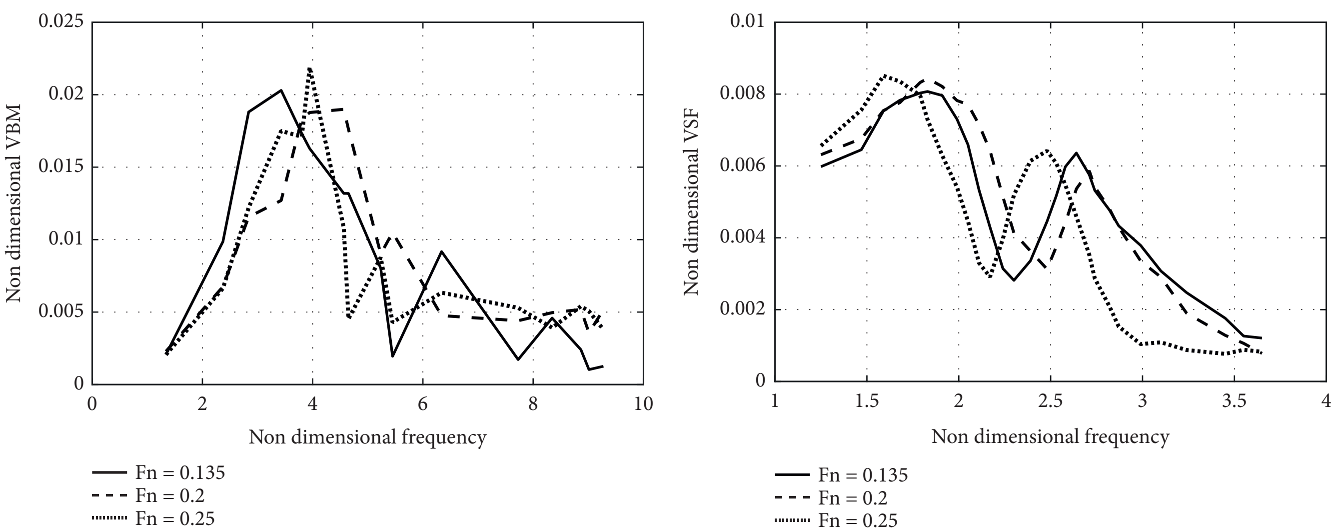

(a) (b)

Figure 13: (a) Transfer function for VBM at amidships for different forward speeds of ULC. (b) Transfer function for VSF at amidships for different forward speeds of ULC.

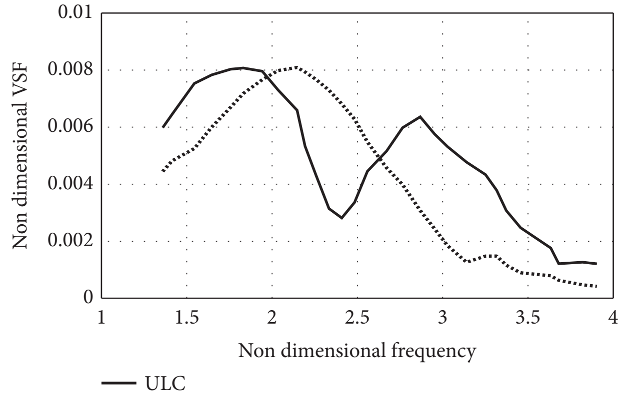

Figure 14: Shear force RAO comparison between S175 and the ULC ($F_n = 0.135$).

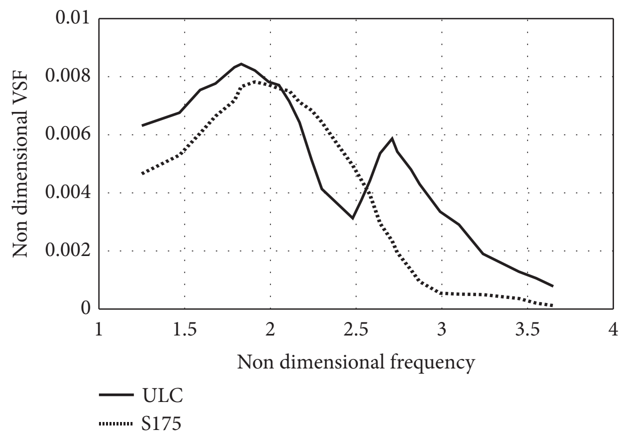

Figure 15: Shear force RAO comparison between S175 and the ULC ($F_n = 0.2$).

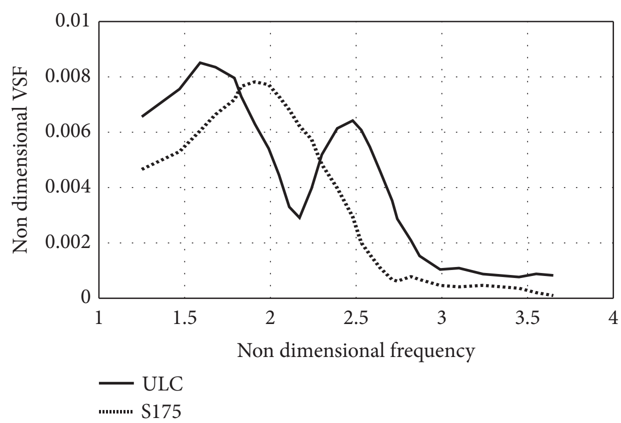

Figure 16: Shear force RAO comparison between S175 and the ULC ($F_n = 0.25$).

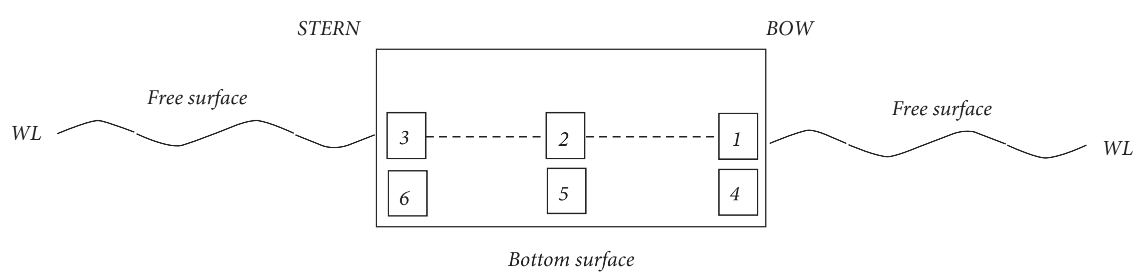

Figure 17: Schematic diagram of selection of panels (squares 1–3 highlight free surface locations; 4–6 highlight ship bottom locations).

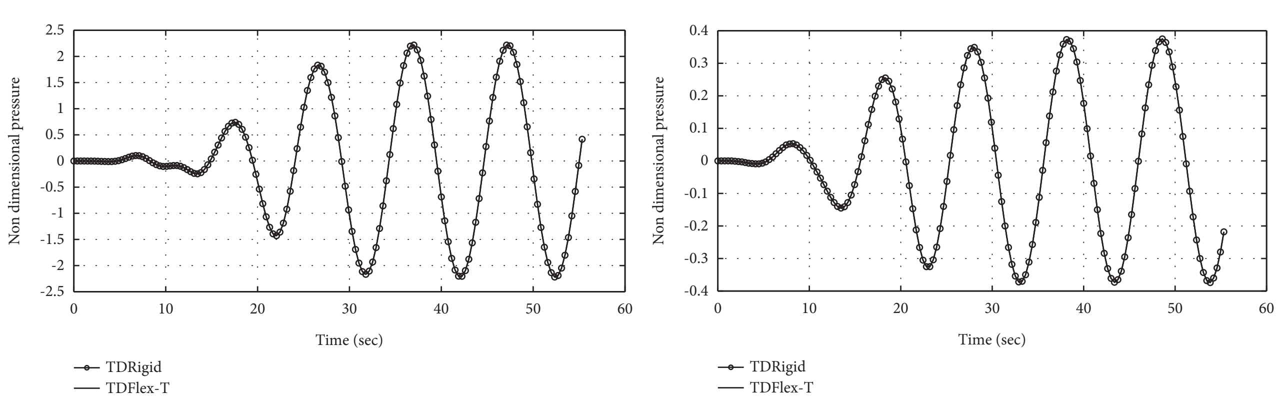

(a)

Figure 18: Continued.

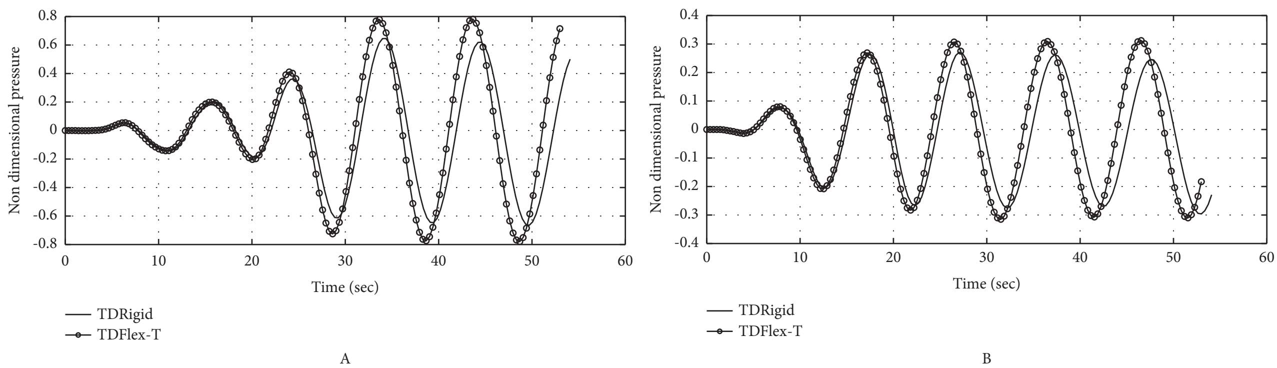

(b)

Figure 18: (a) Pressure time history of S175 hull at bow region, $F_n = 0.25$, $\lambda/L = 1$. (A) Pressure on free surface (see Figure 17; location point 1). (B) Pressure on bottom surface (see Figure 17; location point 4). (b) Pressure time history of ULC at bow region, $F_n = 0.25$, $\lambda/L = 1$. (A) Pressure at free surface (Figure 17; location point 1). (B) Pressure at bottom surface (Figure 17; location point 4).

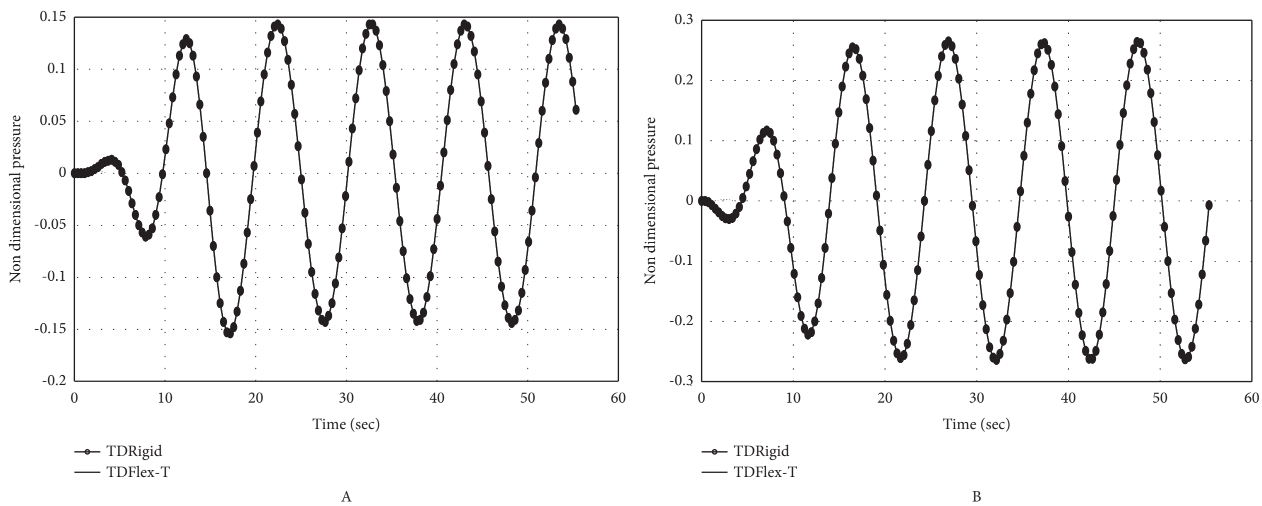

(a)

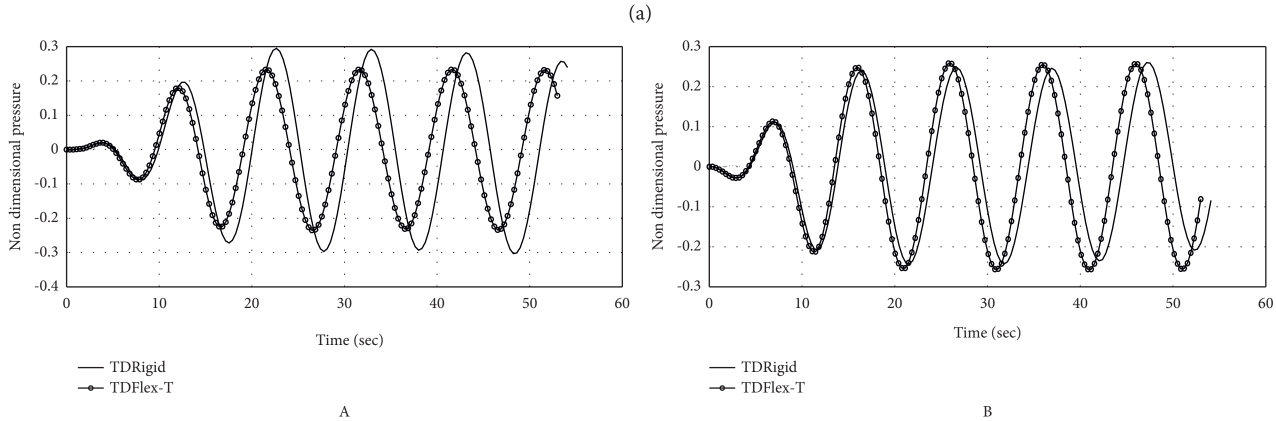

(b)

Figure 19: (a) Pressure time history of S175 hull at midship region, $F_n = 0.25$, $\lambda/L = 1$. (A) Pressure at free surface (Figure 17; location point 2). (B) Pressure at bottom surface (Figure 17; location point 5). (b) Pressure time history of ULC at midship region, $F_n = 0.25$, $\lambda/L = 1$. (A) Pressure at free surface (Figure 17; location point 2). (B) Pressure at bottom surface (Figure 17; location point 5).

and 18(b) display the pressure time histories in way of the bow region of both ships (Figure 17; location points 1 and 4). It is shown that the influence of flexibility is significant only for the ULC container ship model. This trend is confirmed by the comparisons shown in Figures 19(a), 19(b), 20(a), 20(b), respectively, corresponding to responses in way of

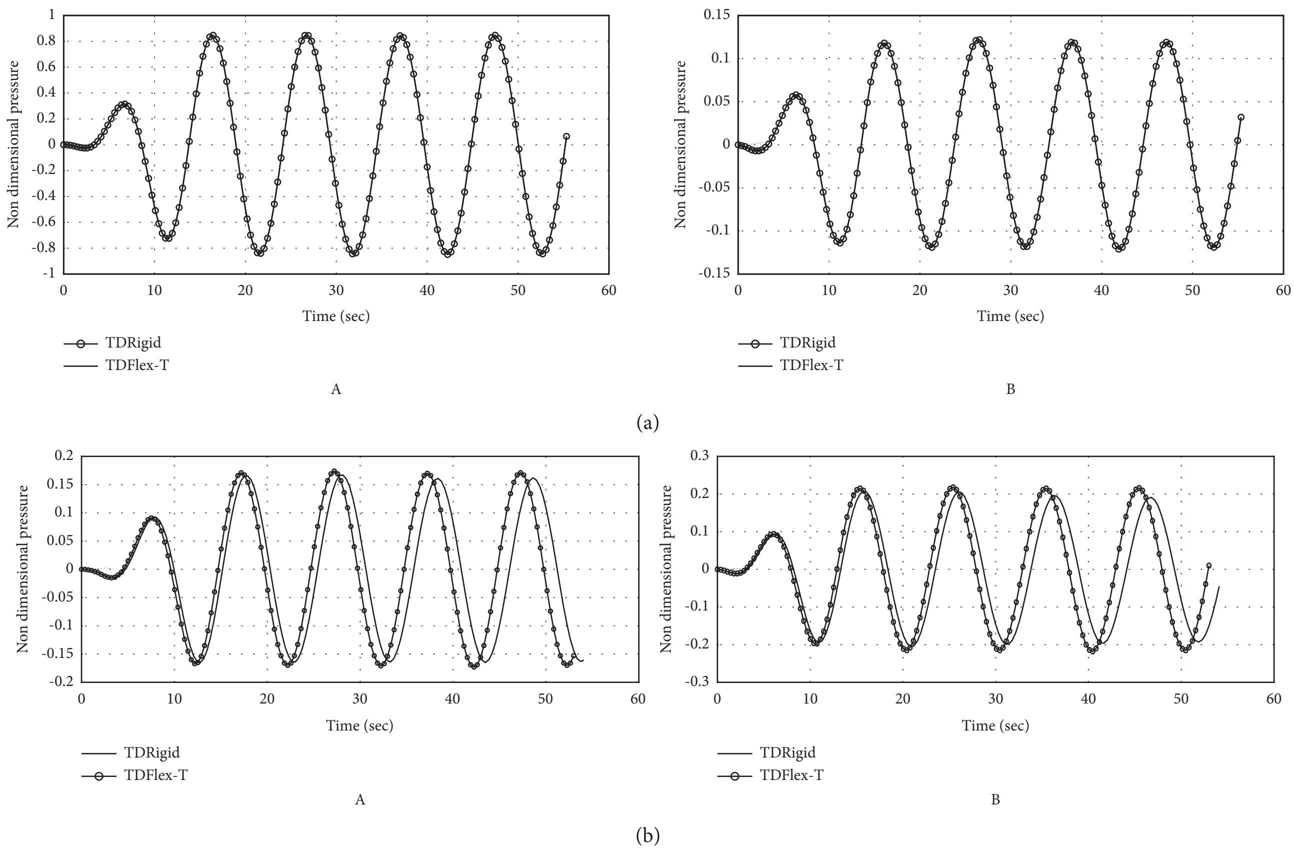

FIGURE 20: (a) Pressure time history of S175 hull at stern region, $F_n = 0.25$, $\lambda/L = 1$. (A) Pressure at free surface (Figure 17; location point 3). (B) Pressure at bottom surface (Figure 17, location point 6). (b) Pressure time history of S175 hull at stern region, $F_n = 0.25$, $\lambda/L = 1$. (A) Pressure at free surface (Figure 17; location point 3). (B) Pressure at bottom surface (Figure 17; location point 6).

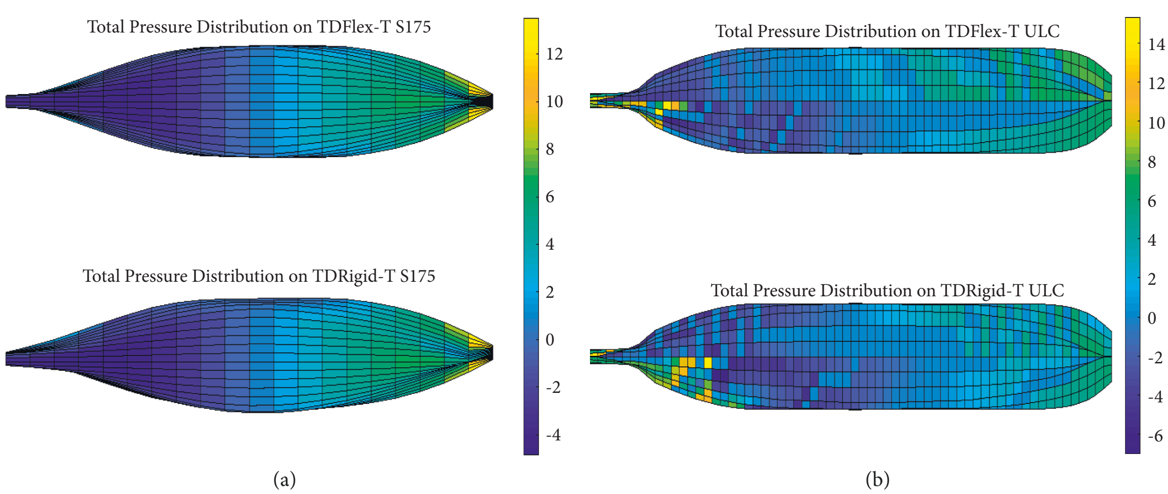

FIGURE 21: (a) Contour plot of pressure profile for a particular instant of time of S175 ship, $F_n = 0.25$, $\lambda/L = 1$. (b) Contour plot of pressure profile for a particular instant of time of ULC, $F_n = 0.25$, $\lambda/L = 1$.

amidships (see Figure 17; location points 2 and 5) and astern (see Figure 17; location points 3 and 6). The variation of the pressure along the ship hull for a particular time instant is depicted in Figures 21(a) and 21(b). The same plots display that the pressure variation is more visible for the case of ULC. It may be therefore concluded that as the ship length increases, the influence of hull flexibility on hydrodynamic pressures becomes prominent.

5. Conclusions

This paper presented a direct hydroelastic analysis method that combines a time-domain Green function with Timoshenko beam structural dynamics for the prediction of symmetric ship responses in waves. The hydrodynamic model is based on the linear 3D time-domain panel method where the Timoshenko beam model is adopted for the structural solution. Results were validated by comparisons against a range of available experimental data. A parametric study for three different containership hull forms demonstrated that hull slenderness and forward speed may influence symmetric flexible ship responses. Future research will focus on developing a fully nonlinear hydroelastic method for the prediction of extreme sea loads (e.g., slamming, green water on decks, and so on) on hull forms of low rigidity progressing at a medium to high speed in irregular waves.

Nomenclature

English symbols

A: Wave amplitude (m)
E: Young's modulus (N/m^2)
I: Moment of inertia (kg-m^2)
F_n: Froude number
f: Sectional load (N/m)
G: Shear modulus (N/m^2)
$G(x_s y_s z_s)$: Ship centre of gravity
g: Acceleration of gravity (m/sec^2)
K_{ij}: Global stiffness factor
k_s: Shear correction factor
L: Hull length (m)
M: Vertical bending moment (N-m)
$Oxyz$: Vessel Earth fixed coordinate system in way of the centre of gravity
p: Field point
q: Source point
S_0: Mean wetted surface
T: Time period (sec)
t: Time (sec)
U: Forward speed (m/s)
V: Vertical shear force (N)
w: Transverse deflection (m)
x_3: Vertical displacement (m)

Greek symbols

α^b, β^s: Residual weight functions
λ: Wavelength (m)
ρ: Structural density (kg/m^3)
ρ_o: Water density (kg/m^3)
ψ: Bending rotation (rad)
ω: Wave frequency (Hz).

Data Availability

The data supporting this study are original results from computer codes developed by the authors. The comparisons against these data can be found in the open scientific literature, and these comparisons are well justified.

Conflicts of Interest

The authors declare that they have no conflicts of interest.

References

[1] K. H. Shin, J. W. Jo, S. E. Hirdaris et al., "Two- and three-dimensional springing analysis of a 16,000 TEU container ship in regular waves," *Ships and Offshore Structures*, vol. 10, no. 5, pp. 498–509, 2015.

[2] S. E. Hirdaris, N. J. White, N. Angoshtari, M. C. Johnson, Y. Lee, and N. Bakkers, "Wave loads and flexible fluid-structure interactions: current developments and future directions," *Ships and Offshore Structures*, vol. 5, no. 4, pp. 307–325, 2010.

[3] S. E. Hirdaris, W. Bai, D. Dessi et al., "Loads for use in the design of ships and offshore structures," *Ocean Engineering*, vol. 78, pp. 131–174, 2014.

[4] Y. Lee, Z. Wang, WhiteN, and S. Hirdaris, *Time Domain Analysis of Springing and Whipping Response Acting on a Large Container Ship, ASME 2011 30th International Conference on Ocean, Offshore and Arctic Engineering OMAE2011-49218*, Rotterdam, The Netherlands, 2011.

[5] R. E. D. Bishop and W. G. Price, *Hydroelasticity of Ships*, Cambridge University Press, Cambridge, United Kingdom, 1979.

[6] R. E. D. Bishop, W. G. Price, and Y. Wu, "A general linear hydroelasticity theory of floating structures moving in a seaway, Philosophical Transactions of the Royal Society of London. Series A," *Mathematical and Physical Sciences*, vol. 316, pp. 375–426, 1986.

[7] S. E. Hirdaris, W. G. Price, and P. Temarel, "Two-and three-dimensional hydroelastic modelling of a bulker in regular waves," *Marine Structures*, vol. 16, no. 8, pp. 627–658, 2003.

[8] S. Malenica, B. Molin, and I. Senjanociv, "Hydroelastic response of a barge to impulsive and non-impulsive wave loads," in *Proceedings of the 3rd International Conference on Hydroelasticity in Marine Technology*, Oxford, United Kingdom, 15th - 17th September 2003.

[9] S. Malenica, I. Senjanovic, and S. Tomasevic, *An Efficient Hydroelastic Model for Wave Induced Coupled Torsional and Horizontal Ship Vibrations*, IWWWFB, Loughborough, UK, 2006.

[10] S. E. Hirdaris, *Hydroelastic Modelling: Prediction of Wave Loads on Bulk Carriers*, VDM Verlag Dr. Müller, Saarbrucken, Germany, 2009.

[11] R. D. Harding, S. E. Hirdaris, S. H. Miao, M. Pittilo, and P. Temarel, "Use of hydroelasticity analysis in design," in *Proceedings of the 4th International Conference on Hydroelasticity in Marine Technology*, pp. 1–12, National Defense Industry Press, Wuxi, China, 10 – 14 September 2006.

[12] P. Temarel and S. E. Hirdaris, Eds., *Hydroelasticity 2009: Hydroelasticity in Marine Technology*, p. 405pp, University of Southampton, Southampton, UK, 2009.

[13] S. E. Hirdaris and P. Temarel, "Hydroelasticity of ships: recent advances and future trends," *Proceedings of the Institution of Mechanical Engineers - Part M: Journal of Engineering for the Maritime Environment*, vol. 223, no. 3, pp. 305–330, 2009.

[14] I. Senjanović, N. Vladimir, M. Tomić, N. Hadzic, and Š Malenica, "Global hydroelastic analysis of ultra large container ships by improved beam structural model," *International J on Nav. Archit. Ocean Engineering*, vol. 6, pp. 1041–1063, 2014.

[15] O. Belik, R. Bishop, and W. Price, "A simulation of ship responses due to slamming in irregular head waves," *Trans. of RINA*, vol. 125, pp. 237–253, 1983.
[16] R. Bishop, J. D. Clarke, and W. G. Price, "Comparison of full scale and predicted responses of two frigates in severe weather trial," *Trans. RINA*, vol. 126, pp. 123–166, 1984.
[17] C. Guedes Soares, "Transient response of ship hulls to wave impact," *International Shipbuilding Progress*, vol. 36, pp. 137–156, 1989.
[18] M. K. Wu and O. A. Hermundstad, "Time domain simulation of wave-induced nonlinear motions and loads and its applications in ship design," *Marine Structures*, vol. 15, pp. 561–597, 2002.
[19] P. A. K. Lakshmynarayanana and S. Hirdaris, "Comparison of nonlinear one- and two-way FFSI methods for the prediction of the symmetric response of a containership in waves," *Ocean Engineering*, vol. 203, Article ID 107179, 2020.
[20] J. Jiao, S. Huang, and C. G. Soares, "Viscous fluid–flexible structure interaction analysis on ship springing and whipping responses in regular waves," *Journal of Fluids and Structures*, vol. 106, Article ID 103354, 2021.
[21] T. Hamamoto, A. Suzuki, N. Tsujioka, and K.-i. Fujita, "3D BEM-FEM hybrid hydroelastic analysis of module linked large floating structures subjected to regular waves," in *The Eighth International Offshore and Polar Engineering Conference*International Society of Offshore and Polar Engineers, Montreal, Quebec, Canada, 1998.
[22] X. D. Liu and S. Sakai, "Time domain analysis on the dynamic response of a flexible floating structure to waves," *J. Eng. Mechanics-Asce*, vol. 128, no. 1, pp. 48–56, 2002.
[23] J. H. Kyoung, S. Y. Hong, and B. W. Kim, "FEM for time domain analysis of hydroelastic response of VLFS with fully nonlinear free-surface conditions," *International Journal of Offshore and Polar Engineering*, vol. 16, no. 3, pp. 168–174, 2006.
[24] Q. C. Liuchao and L. Hua, "Three-dimensional time-domain analysis of very large floating structures subjected to unsteady external loading," *J. Offshore Mech. Arct. Eng. Trans. Asme*, vol. 129, no. 1, pp. 21–28, 2007.
[25] J. H. Kim and Y. Kim, "Numerical analysis on springing and whipping using fully-coupled FSI models," *Ocean Engineering*, vol. 91, pp. 28–50, 2014.
[26] Y. Kim, K. H. Kim, and Y. Kim, "Analysis of hydroelasticity of floating ship like structure in time domain using a fully coupled hybrid BEM-FEM," *Journal of Ship Research*, vol. 53, no. 1, pp. 31–47, 2009a.
[27] Y. Kim, K. H. Kim, and Y. Kim, "Springing analysis of a seagoing vessel using fully coupled BEM-FEM in the time domain," *Ocean Engineering*, vol. 36, no. 11, pp. 785–796, 2009b.
[28] Y. Kim, K. H. Kim, and Y. Kim, "Time domain springing analysis on a floating barge under oblique wave," *Journal of Marine Science and Technology*, vol. 14, no. 4, pp. 451–468, 2009c.
[29] J. H. Kim, Y. Kim, R. H. Yuck, and D. Y. Lee, "Comparison of slamming and whipping loads by fully coupled hydroelastic analysis and experimental measurement," *Journal of Fluids and Structures*, vol. 52, pp. 145–165, 2015.
[30] K. H. Kim and Y. Kim, "Springing analysis of a seagoing vessel using fully coupled BEM–FEM in the time domain," *Ocean Engineering*, vol. 36, pp. 785–796, 2009.
[31] F. Kara, "Time domain prediction of hydroelasticity of floating bodies," *Applied Ocean Research*, vol. 51, pp. 1–3, 2015.
[32] H. Y. Kang and M. H. Kim, "Time-domain hydroelastic analysis with efficient load estimation for random waves," *International Journal of Naval Architecture and Ocean Engineering*, vol. 9, no. 3, pp. 266–281, 2017.
[33] S. Rajendran and C. Guedes Soares, "Numerical investigation of the vertical response of a containership in large amplitude waves," *Ocean Engineering*, vol. 123, pp. 440–451, 2016.
[34] D. H. Lee and H. S. Choi, "Transient hydroelastic response of very large floating structures by FE-BE hybrid method," in *Proceedings of the The Thirteenth International Offshore and Polar Engineering Conference*, Honolulu, Hawaii, USA, 2003.
[35] M. Kashiwagi, "A B-spline Galerkin scheme for calculating the hydroelastic response of a very large floating structure in waves," *Journal of Marine Science and Technology*, vol. 3, no. 1, p. 37e49, 1998a.
[36] M. Kashiwagi, "A direct method versus a mode-expansion method for calculating hydroelastic response of a VLFS in waves," in *Proceedings of the The Eighth International Offshore and Polar Engineering Conference*, Montreal, Quebec, Canada, 1998b.
[37] R. Taghipour, T. Perez, and T. Moan, "Time-domain hydroelastic analysis of a flexible marine structure using state-space models," *Journal of Offshore Mechanics and Arctic Engineering*, vol. 131, no. 1, 2009.
[38] J. Jiao, H. Yu, C. Chen, and H. Ren, "Time domain numerical and segmented model experimental study on ship hydroelastic responses and whipping loads in harsh irregular seaways," *Ocean Engineering*, vol. 185, pp. 59–81, 2019.
[39] J. Jiao, Z. Chen, C. Chen, and H. Ren, "Time domain hydroelastic analysis of nonlinear motions and loads on a large bow-flare ship advancing in high irregular seas," *Journal of Marine Science and Technology*, vol. 25, pp. 426–454, 2020.
[40] S. Pal, R. Datta, and M. R. Sunny, "Fully coupled time domain solution for hydroelastic analysis of floating boy," *Ocean Engineering*, vol. 153, pp. 173–184, 2018.
[41] R. Datta and C. Guedes Soares, "Analysis of the hydroelastic effect on a container vessel using coupled BEM–FEM method in the time domain," *Ships and Offshore Structures*, vol. 15, no. 4, pp. 393–402, 2020.
[42] Y. Lee, N. White, Z. Wang, S. Zhang, and S. Hirdaris, "Comparison of springing and whipping responses of model tests with predicted nonlinear hydroelastic analyses," *International Journal of Offshore and Polar Engineering*, vol. 22, no. 3, p. 209, 2012.
[43] J. H. Kim, Y. Kim, and A. Korobkin, "Comparison of fully coupled hydroelastic computation and segmented model test results for slamming and whipping loads," *Int. J. Naval Architect. Ocean Eng.*vol. 6, pp. 1064–1081, 2014.
[44] K. H. Kim, B. W. Kim, and S. Y. Hong, "Experimental investigations on extreme bow-flare slamming loads of 10,000-TEU containership," *Ocean Engineering*, vol. 171, pp. 225–240, 2018.
[45] J. L. Jiao, H. L. Ren, and C. H. Chen, "Model testing for ship hydroelasticity: a review and future trends," *Journal of Shanghai Jiao Tong University*, vol. 22, pp. 641–650, 2017.
[46] S. E. Hirdaris, Y. Lee, G. Mortola et al., "The influence of nonlinearities on the symmetric hydrodynamic response of a 10,000 TEU container ship," *Ocean Engineering*, vol. 111, pp. 166–178, 2016.
[47] P. Yang, W. Zhang, X. Wang et al., "Uncertainty analysis of hydroelastic responses and wave loads for different structural modeling and potential methods," *Ocean Engineering*, vol. 222, Article ID 108529, 2021.

[48] R. Datta and D. Sen, "The simulation of ship motion using a B-spline based panel method in time domain," *Journal of Ship Research*, vol. 51, no. 3, pp. 267–284, 2007.
[49] N. M. Newmark, "A method of computation for structural dynamics," *Journal of Engineering Mechanics Division, Proceedings of the American Society of Civil Engineers*, vol. 85, no. 3, pp. 67–94, 1959.
[50] N. Datta and M. A. Siddiqui, "Hydroelastic analysis of axially loaded Timoshenko beams with intermediate end fixities under hydrodynamic slamming loads," *Ocean Engineering*, vol. 127, pp. 124–134, 2016.
[51] S. E. Hirdaris and A. W. Lees, "A conforming unified finite element formulation for the vibration of thick beams and frames," *International Journal for Numerical Methods in Engineering*, vol. 62, pp. 579–599, 2005.
[52] J. Rakowski, "The interpretation of the shear locking in beam elements," *Computers & Structures*, vol. 37, no. 5, pp. 769–776, 1990.
[53] M. Liu and D. G. Gorman, "Formulation of Rayleigh damping and its extensions," *Computers & Structures*, vol. 57, pp. 277–285, 1995.
[54] Y. Liu, Z. Liu, Q. Song, and B. Wang, "Development of constrained layer damping toolholder to improve chatter stability in end milling," *International Journal of Mechanical Sciences*, vol. 117, pp. 299–308, 2016.
[55] W. M. Lin and D. Yue, "Numerical Solution for large amplitude motions in the time domain," in *Proceedings of the 18th ONR Symposium on Naval Hydrodynamics*, pp. 41–66, National Academy Press, Washington DC, 1990.
[56] A. Cabada, L. López-Somoza, and M. Yousfi, "Green's function related to a n^{th} order linear differential equation coupled to arbitrary linear non-local boundary conditions," *Mathematics*, vol. 9, no. 16, p. 1948, 2021.
[57] J. P. Boin, M. Guilbaud, and M. Ba, *Seakeeping Computations Using the Ship Motion Green Function*, pp. 398–405, ISOPE, Seattle, 2000.
[58] I. Drummen and M. Holtmann, "Benchmark study of slamming and whipping," *Ocean Engineering*, vol. 86, pp. 3–10, 2014.
[59] S. Rajendran, N. Fonseca, and C. Guedes Soares, "A numerical investigation of the flexible vertical response of an ultra large containership in high seas compared with experiments," *Ocean Engineering*, vol. 122, pp. 293–310, 2016.
[60] D. Sengupta, S. K. Pal, and R. Datta, "Hydroelasticity of a 3D floating body using a semi analytic approach in time domain," *Journal of Fluids and Structures*, vol. 71, pp. 96–115, 2017.
[61] K. Iijima, T. Yao, and T. Moan, "Structural response of a ship in severe seas considering global hydroelastic vibrations," *Marine Structures*, vol. 21, no. 4, pp. 420–445, 2008.